Life Sciences 216 (2019) 259–270

Contents lists available at ScienceDirect

Life Sciences

journal homepage: www.elsevier.com/locate/lifescie

Alpinumisoflavone causes DNA damage in Colorectal Cancer Cells *via* blocking DNA repair mediated by RAD51

Dong Li*, Xiaoyan Li, Genqu Li, Yan Meng, Yanghong Jin, Shuang Shang, Yanjie Li

Department of Pharmacy, Puyang Oilfield General Hospital, Henan, China

ARTICLE INFO

Keywords:
Alpinumisoflavone
RAD51
CRC
DNA-strand break
γ-H2AX

ABSTRACT

Aims: Colorectal Cancer (CRC) accounts for 6.1% incidence and 9.2% mortality worldwide. The current study aimed to investigate the effect of alpinumisoflavone (AIF) on CRC and its possible molecular mechanism.

Methods: HCT-116 and SW480 cells were chosen as cell model to study the anti-cancer activity of AIF *in vitro* experiments. Cells proliferative capacity and clonogenicity were examined by CCK-8 assay and colony formation assay, while cell apoptosis was detected by Hoechst 33258 staining and Flow cytometer. The protein expression levels of related gene were examined by western blotting. Transcriptome analyses were conducted to identify the differentially expressed genes in CRC cells, following AIF treatment. DNA damage was examined by γH2AX foci assay. The anti-cancer effect of AIF *in vivo* was validated in CRC xenograft model.

Key findings: We found that AIF inhibited CRC cell proliferation and promoted apoptosis in a dose-dependent manner, as well as increased the number of γ-H2AX foci. In addition, microarray analysis showed that the DNA-double strand break (DSB) repair gene RAD51 was aberrantly overexpressed in CRC tissues, and was positively correlated with lymph node metastasis, TNM stage and poor outcomes. Both *in vitro* and *in vivo* experiments confirm that AIF treatment significantly decreased RAD51 levels. Knockdown RAD51 could enhance the anti-cancer activity of AIF against CRC, while abrogated by RAD51 overexpression.

Significance: These findings suggest that AIF can be regarded as a potential anti-cancer drug and provide new insights into CRC treatment.

1. Introduction

Colorectal Cancer (CRC) is the fourth leading cause of cancer-related deaths worldwide, and remains a serious public health problem [1]. The current treatment options of CRC, such as surgical resection, chemotherapy, and radiotherapy, offer limited survival benefits, and the 5-year mortality rate among the advanced CRC patients is still 50% [2]. Therefore, novel predictive and/or therapeutic biomarkers for CRC are urgently needed.

DNA double-strand breaks (DSBs) are usually triggered by exogenous chemical agents or ionizing radiation [3], and can lead to genetic instability and apoptosis. The lethal consequences of DSBs are alleviated or prevented by two main repair mechanisms: non-homologous end-joining (NHEJ) and homologous recombination (HR) [4]. RAD51, an important mediator of HR repair (HRR), is aberrantly overexpressed in various malignancies and is associated with radio- and chemo-resistance of the tumor cells, which often result in poor outcomes [5]. RAD51 promotes carcinogenesis and progression by interacting with p53, p21 and Bcl-2, and leads to mismatch repair and apoptosis evasion in the pre-malignant cells [5,6]. Following the DSB stimuli, the ataxia telangiectasia mutated (ATM) kinase phosphorylates the hydroxyl terminal of H2AX at the serine-139 residue, which subsequently recruits DNA-repair related proteins and cyclins to the damaged site. Studies show that down-regulating H2AX levels in tumor cells enhances their sensitivity to chemo- and radiotherapy [7,8]. Taken together, targeting RAD51 and H2AX can potentially sensitize tumor cells to radio- and chemotherapy, and induce apoptosis.

High-throughput screening of small-molecule libraries has helped discover numerous novel chemotherapeutic agents, including paclitaxel, camptothecin, Vinca alkaloids and their derivatives *etc.* [9]. In recent decades, the focus of anti-cancer drug discovery has shifted to screening for the bioactive ingredients in natural products because of their lower toxicity and higher efficacy [10]. Alpinumisoflavone (AIF), the principal bioactive component isolated from *D. eriocarpa*, a traditional Chinese medicine herb, has potent pharmacological properties, including atheroprotective [11], molluscicidal [12], estrogenic [13], and anti-bacterial activities [14]. Zhang et al. reported that AIF enhanced the sensitivity of esophageal squamous cell carcinoma (ESCC)

* Corresponding author at: No.124 Daqing Road, Puyang, Henan 457001, China.
E-mail address: donglipyhn@163.com (D. Li).

https://doi.org/10.1016/j.lfs.2018.11.032
Received 28 September 2018; Received in revised form 7 November 2018; Accepted 15 November 2018
Available online 16 November 2018
0024-3205/

Table 1
The correlation between RAD51 expression and clinicopathological characteristics of included patients.

Variables	RAD51 expression		*p* value
	High (27)	Low (20)	
Age			0.8622
≤50	14	8	
> 50	19	12	
Sex			0.9426
Male	20	15	
Female	7	5	
Tumor size			0.1188
≤5 cm	10	12	
> 5 cm	17	8	
TNM stage			0.0315*
I and II	9	13	
III and IV	18	7	
Site			0.8307
Colon	13	9	
Rectum	14	11	
Lymph node metastasis			0.0254*
Absence	17	6	
Presence	10	14	

* $p < 0.05$.

cells to radiotherapy by inducing cell cycle arrest and apoptosis [15]. In addition, AIF has also shown anti-neoplastic activity in lung cancer [16], renal cell carcinoma [17], and melanoma [18].

The aim of this study was to determine the potential anti-cancer effect of AIF on CRC cells. We found that AIF inhibited CRC cell growth and triggered apoptosis in a dose-dependent manner by inducing DNA DSBs and blocking DNA damage repair, as evidenced by RAD51 down-regulation and increased γH2AX foci in the CRC cells. Furthermore, inhibition of RAD51 *in vitro* augmented the anti-cancer effects of AIF. Taken together, AIF suppressed CRC cell growth by modulating RAD51.

2. Materials and methods

2.1. CRC tissue samples

In present study, all investigation and experiments have obtained patients' consent and been approved by the Ethic Committee of Puyang Oilfield General Hospital (Henan, China). Resected 47 pairs CRC tumors tissues and adjacent non-tumor tissues were sampled from a total of 47 patients in Puyang Oilfield General Hospital from Jan 2011 to March 2013. Diagnosis and staging were carried out by 2 independent senior oncologists blinded to the data. The level of RAD51 in tissue samples was determined by immunohistochemical assay. According to the percentage of positively stained cells, the sections were graded by five levels: 0 (≤5%), 1 positive cells and the staining intensity were multiplied to generate an immune-reactive score for each specimen (0 − 12). Based on the total score, scores of 0–3 were considered as the low expression group, and scores of 4–12 were defined as the high expression group. All the patients were followed up by telephone up to April 30, 2018, to obtain the survival data. The correlation between RAD51 expression and clinicopathological characteristics of included patients was listed in Table 1.

2.2. Antibodies and reagents

Antibodies against RAD51 (#88572, 1 μg/ml), phospho-γ-H2AX (#2893, 1:1000), pro-caspase-3 (#32150, 1:1000), cleaved caspase-3 (#2302, 1 μg/ml), Bax (#32503, 1:1000) and Bcl-2 (#196495, 1:1000) were purchased from Abcam (Cambridge, MA, USA). HRP-labelled goat anti-rabbit IgG (#A0208, 1:1000) and anti-mouse IgG (#A0216, 1:1000), and anti-GAPDH were obtained from Beyotime Biotechnology (Shanghai, China). Alpinumisoflavones (CFN98440, 10 mg, HPLC ≥ 95%) was purchased from chemFaces (Wuhan, China).

2.3. Cell lines and culture

Two well-established CRC cell lines, HCT-116 (#CCL-247) and SW480 (#CCL-228) cells were purchased from the American Type Culture Collection. Cells were cultured in McCoy's 5a medium (HCT-116) or L-15 medium (SW480) containing 10% fetal bovine serum at 37 °C under 5% CO_2.

2.4. Cell proliferation assay

The viability of CRC cells treated with AIF was analyzed using the CCK-8 kit (#C0038, Beyotime Biotechnology, Shanghai, China) according to the manufacturer's instructions. Briefly, 5×10^3 CRC cells were seeded in 96-well plates and stimulated with different concentrations of AIF for the indicated durations. The culture medium was replaced with 100 μl fresh medium containing 10 μl CCK-8 reagent per well, and the cells were incubated further for 2 h. The absorbance at 450 mm was measured using a microplate reader (Multiskan FC, ThermoFisher, Waltham, MA).

2.5. Colony formation assay

HCT-116 and SW480 cells were seeded into 6-well plates at the density of 300 cells/well and cultured with different concentrations of AIF or the vehicle for 14 days. The ensuing colonies were fixed with 4% paraformaldehyde (#P0099, Beyotime Biotechnology, Shanghai, China) for 15 min and stained with 1% crystal violet (#C0121, Beyotime Biotechnology, Shanghai, China) for 10 min as previously described [19]. The number of colonies were counted in five randomly chosen fields under an inverted microscope (40×), and the colony-forming efficiency was calculated as the number of colonies/500 × 100%.

2.6. Hoechst 33258 staining

Chromatin condensation in HCT-116 and SW480 cells was determined using Hoechst 33258 staining. Briefly, 1×10^5 cells were seeded per well in 6-well plates and cultured with AIF or the vehicle for 48 h. The cells were fixed with 4% paraformaldehyde for 15 min at room temperature, and stained with Hoechst 33258 (#C1017, Beyotime Biotechnology, Shanghai, China) according to the manufacturer's instructions. The cells were observed under a fluorescence microscope (Olympus Corporation, Tokyo, Japan).

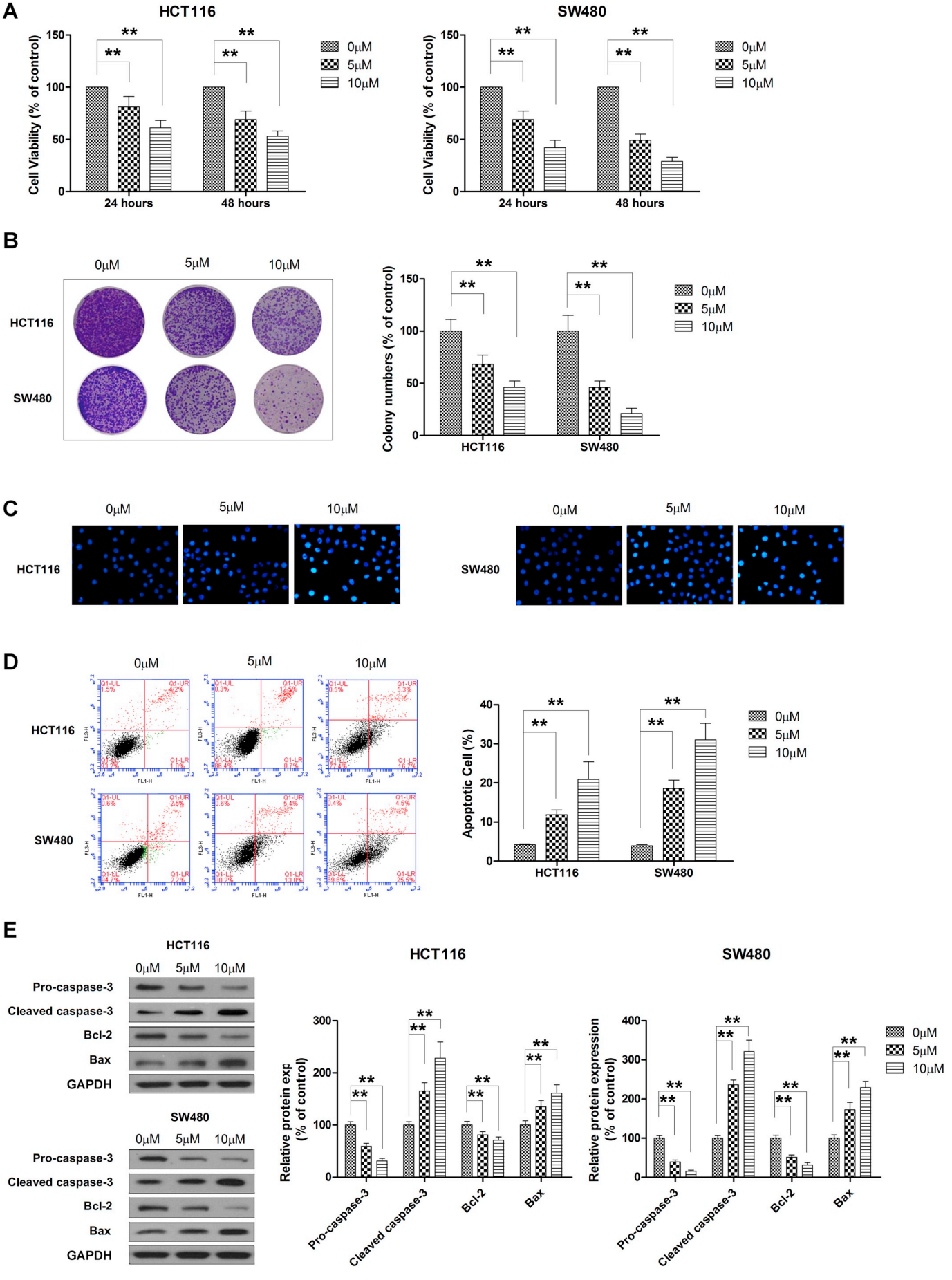

(caption on next page)

Fig. 1. AIF induces apoptosis in CRC cells. A. HCT-116 and SW480 cells were treated with AIF (5 and 10 μM) for 24 h and 48 h, and viability was determined by CCK-8 assay. B. Colony formation assay of HCT-116 and SW480 cells treated with AIF (5 and 10 μM) for the indicated durations. (C, D). AIF-treated cells were stained with Hoechst 33258 and percentage of apoptotic cells was measured using flow cytometry. E. Western blot showing the relative levels of the apoptosis-associated proteins pro-caspase-3, caspase-3, Bcl-2 and Bax normalized to GAPDH. Data are presented as mean ± SD from three independent experiments, $^{**}p < 0.01$.

2.7. Annexin V-FITC/PI staining

Apoptosis in the CRC cells was determined by Annexin V/PI staining as previously described [20]. Briefly, 2×10^5 cells were seeded per well in 6-well plates and cultured with various concentrations of AIF for 48 h. The cells were then stained with Annexin V-FITC/PI kit (#C1062, Beyotime Biotechnology Shanghai, China) according to the manufacturer's instructions. The percentage of apoptotic cells were analyzed by flow cytometry (Beckman Coulter Inc., Miami, FL, USA).

2.8. Immuno-fluorescence staining

HCT-116 and SW480 cells were seeded into 24-well plates, with each well containing a glass coverslip, at the density of 2×10^4 cells/well. Following incubation with different concentrations of AIF for the indicated durations, the coverslips were retrieved and air-dried, and the adherent cells were fixed with 2% paraformaldehyde for 30 min. The cells were rinsed in TBS, permeabilized with methanol at −20 °C for 1 min, and rinsed again before blocking with 1% bovine serum albumin (BSA) and 0.2% Tween-20 (TTN) in TBS for 20 min. The cells were then incubated for 2 h with anti-p-γH2AX (Ser-139) mAb (1:500 in TTN; Upstate, Lake Placid, NY). The coverslips were washed and incubated with FITC conjugated anti-mouse goat F (ab′) 2 fragment (1:200 in TTN; DAKO, Carpinteria, CA) for 1 h at room temperature. After rinsing the coverslips, they were immersed in 0.05 mg/ml DAPI for 15 min, rinsed again, and mounted using 10 μl Fluorogard (Bio-Rad) and sealed. Eight hundred randomly selected cells were counted per sample, and cells with three or more γH2AX foci of any size were classified as positive.

2.9. Western blotting

The expression level of specific proteins was evaluated by Western blotting as previously described [21]. Briefly, following 48 h treatment with AIF, the cells were lysed and the protein concentration in the cell lysates was measured. Equal amounts of proteins per sample were resolved by sodium dodecyl sulfate-polyacrylamide gel electrophoresis (SDS-PAGE), and transferred to polyvinylidene fluoride (PVDF) membranes. The blots were subsequently incubated overnight with the primary antibodies against RAD51, γH2AX, pro-caspase-3, cleaved caspase-3, Bax, Bcl-2 and GAPDH (internal control) at 4 °C. After incubation with peroxidase-conjugated secondary antibodies, the immuno-reactive bands were visualized by enhanced BeyoECL Star (no. P0018AM, Beyotime Biotechnology Shanghai, China) according to the manufacturer's instructions.

2.10. Proteomics analysis

iTRAQ-based proteomics analysis was quantitatively analyzed by Shanghai OE Biotech (Shanghai, China) as described previously [22]. In briefly, Following AIF treatment, cells were dissolved in lysis buffer and labelled with iTRAQ labelling reagents. The samples were subjected to LC analysis and tandem mass spectrometry analysis. Protein identification and relative iTRAQ quantification service were provided by Oebiotech (Shanghai, China). The cutoff value for the differentially expressed proteins was adjusted to $p < 0.05$ and the fold change was set to > 1.5 or < 0.5.

2.11. In vivo CRC xenograft model establishment

The Institutional Animal Care and Use Committee at Puyang Oilfield General Hospital approved all animal experiments in this study. Eight week-old male athymic BALB/c nu/nu mice were housed in pathogen-free conditions and given sterile food and water *ad libitum*. After acclimatization, the mice were each injected with 10^7 HCT-116 cells in their left flanks. Twenty-one days after implantation, the mice were randomized into 3 groups (6 mice/group) and injected i.p. as follows: (i) vehicle (0.9% sodium chloride plus 1% dimethyl sulfoxide (DMSO), (ii) AIF (25 mg/kg/day dissolved in vehicle), and (iii) AIF (50 mg/kg/day). The body weight pf the mice and the tumor volume were measured twice every week until the 24th day. The mice were sacrificed and the tumors were resected and weighed. The tumor tissues were processed for histopathological evaluation by hematoxylin and eosin (H &E) staining. *In situ* apoptosis in the tumor tissues was analyzed by TUNEL staining (Biyuntian, Wuxi, China) according to the manufacturer's instructions.

2.12. Statistical analysis

Data are presented as means ± SD from three independent experiments. All statistical analyses were performed using GraphPad Prism 7.0 and SPSS 17.0 software. One-way ANOVA followed by Dunnett's *t*-test was used to compare multiple groups. The relationship between RAD51 levels and the overall survival of CRC patients was analyzed by Kaplan-Meier and log-rank test. A p value < 0.05 was considered statistically significant.

3. Results

3.1. AIF inhibits CRC cell proliferation and promotes apoptosis

The anti-cancer effect of AIF was tested on two well established CRC cell lines, HCT-116 and SW480. The viability of both lines was significantly reduced following exposure to AIF in a time and dose dependent manner, compared to the vehicle control group (Fig. 1A). Consistent with above results, fewer colonies were formed by the AIF-treated cells compared to the control cells (Fig. 1B). Since chromatin condensation is a hallmark of apoptosis [23], we stained the cells with the DNA-specific Hoechst 33258. As shown in Fig. 1C, a significantly higher number of AIF-treated cells had chromatin condensation compared to the vehicle group. In addition, Annexin V/PI staining showed that AIF increased the percentage of apoptotic cells in a dose dependent manner – from 5.2% (HCT-116) and 4.7% (SW480) in the vehicle group to 13.2% and 19.2% in the 5 μM AIF-treated cells, and 22% and 30% in the 10 μM AIF-treated cells (Fig. 1D). Interestingly, the SW480 cells

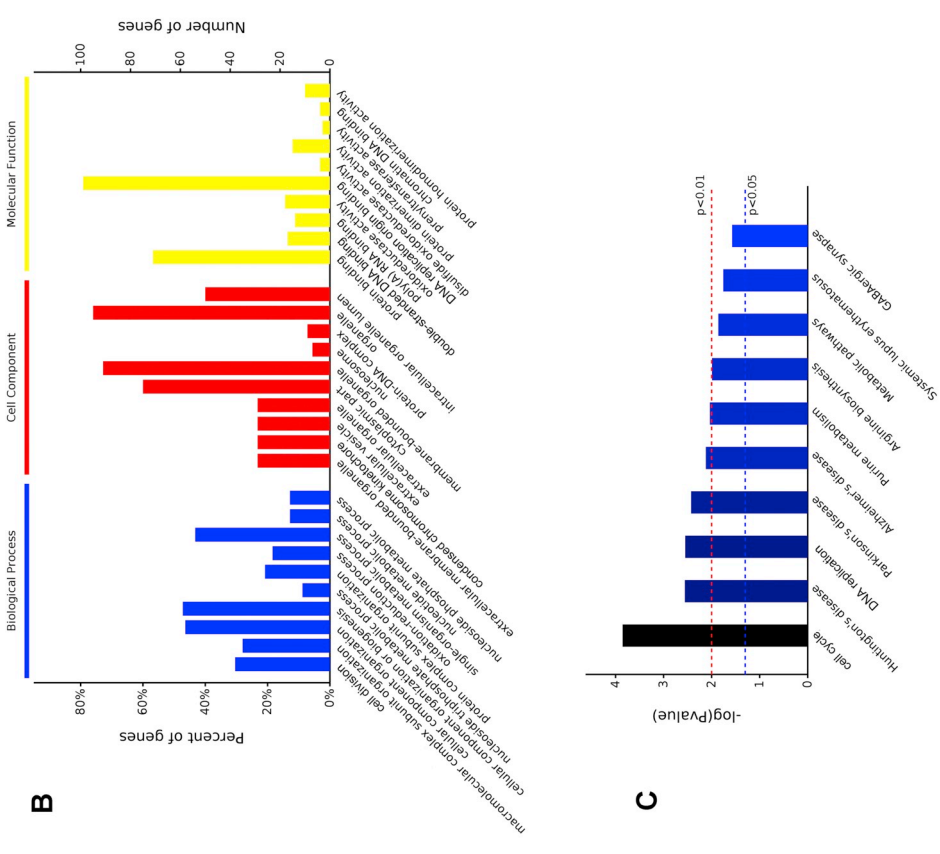

Fig. 2. iTRAQ-based proteomics analysis screening of the differentially expressed genes (DEGs) in AIF or vehicle-treated CRC cells. A. Unsupervised clustering of CRC cells based on the expression pattern of DEGs. B. The functional annotation and classification of the DEGs in AIF or vehicle-treated CRC cells. C. Identification of the cellular functions of DEGs.

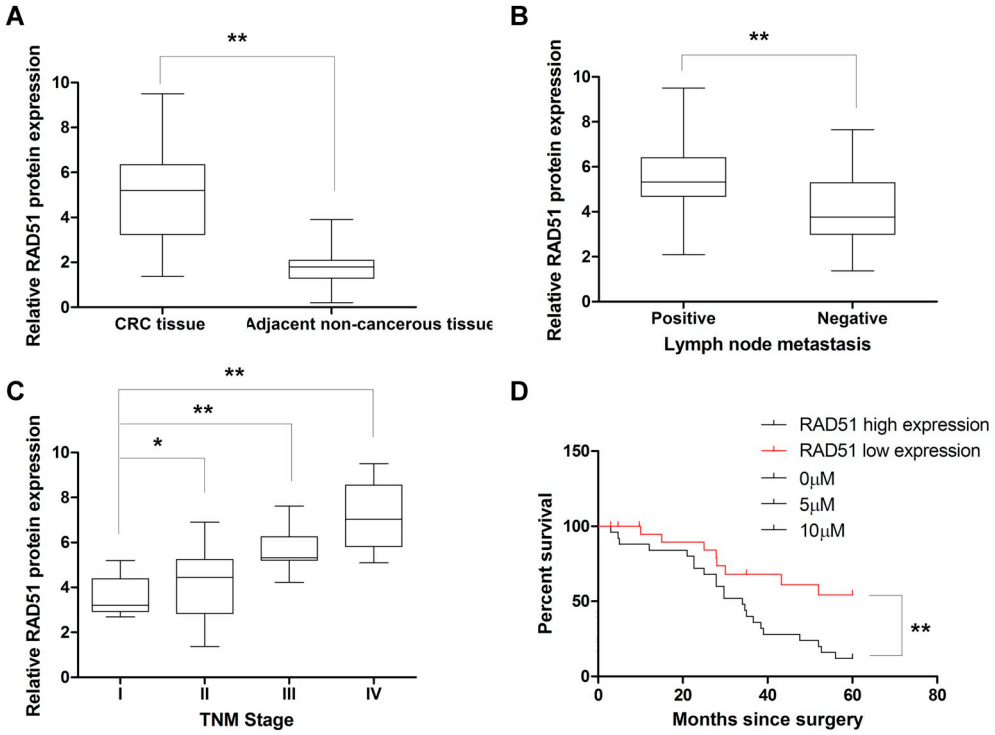

Fig. 3. RAD51 was elevated in CRC tissues and associated with clinico-pathological features. A. RAD51 mRNA was up-regulated in CRC tissues compared to matched non-cancerous tissues. (B–D). RAD51 expression was positively correlated with lymph node metastasis, TNM stage, and poor outcomes.

were more sensitive to AIF-mediated apoptosis compared to the HCT-116 cells. In addition, AIF also upregulated the levels of the pro-apoptotic cleaved caspase-3 and Bax, and downregulated the anti-apoptotic pro-caspase-3 and Bcl-2 proteins (Fig. 1E). Taken together, AIF suppressed proliferation and induced apoptosis in CRC cells.

3.2. AIF alters the transcriptome of CRC cells

To further explore the underlying mechanisms of the anti-proliferative and pro-apoptotic effects of AIF on CRC cells, the transcriptomes of the control and AIF-treated cells were sequenced and the differentially expressed genes (DEGs) were identified. The mRNA expression profiles of the cells are summarized in Fig. 2A, which show that 49 genes were up-regulated and 33 genes were down-regulated in the AIF-treated relative to control cells. The DEGs were then functionally annotated and classified into the biological process, cell component and molecular function groups, which indicated that the most significant DEGs were implicated in cell division and DNA replication (Fig. 2B and C). Therefore, AIF likely exerts its effects in CRC cells by arresting cell cycle and thus altering proliferation rates.

3.3. RAD51 was up-regulated in CRC tissues and associated with poor prognosis in CRC patients

Microarray analysis showed significantly higher abundance of RAD51 in CRC tissues compared to the matched non-cancerous tissues. We validated the microarray results in a relatively large cohort (n = 47) by western blot. As shown in Fig. 3A, RAD1 protein expression levels were ~2.5-fold higher in the CRC tissues compared to the matched healthy tissues. In addition, a positive correlation was observed between RAD51 levels and lymph node metastasis and TNM stage, indicating that RAD51 functions as an oncogene in CRC (Fig. 3B–C, Table 1). Furthermore, high RAD51 levels in CRC tissues were associated with poor overall survival of the patients (Fig. 3D). Taken together, RAD51 is a potential prognostic indicator as well as a therapeutic target for CRC.

3.4. AIF induces DNA-DSBs in CRC cells by down-regulating RAD51

To summarize the results above, CRC tissues had significantly higher RAD1 expression levels, and AIF significantly downregulated RAD51 mRNA in CRC cells. We hypothesized therefore that the inhibitory effect of AIF on CRC cell survival was mediated *via* RAD1 down-regulation. In support of our hypothesis, both 5 and 10 μM AIF effectively decreased the level of RAD51 protein in HCT-116 and SW480 cells (Fig. 4A). Given that RAD51 is involved in DNA DSB repair, we next speculated that AIF blocks RAD51-mediated DNA breakage repair in the CRC cells. DSB formation is characterized by the phosphorylation of H2AX at ser-139 to γ-H2XA, which serves as a reliable marker of DNA damage [24]. As shown in Fig. 4B, few γ-H2AX foci were observed in the vehicle-treated cells, and was dramatically increased upon AIF treatment. In addition, 5 and 10 μM AIF increased the levels of phosphorylated H2AX by 1.8 and 2.8-folds respectively compared to that in the control cells (Fig. 4C). Taken together, AIF increases DNA DSBs by inhibiting DNA repair *via* RAD51 down-regulation.

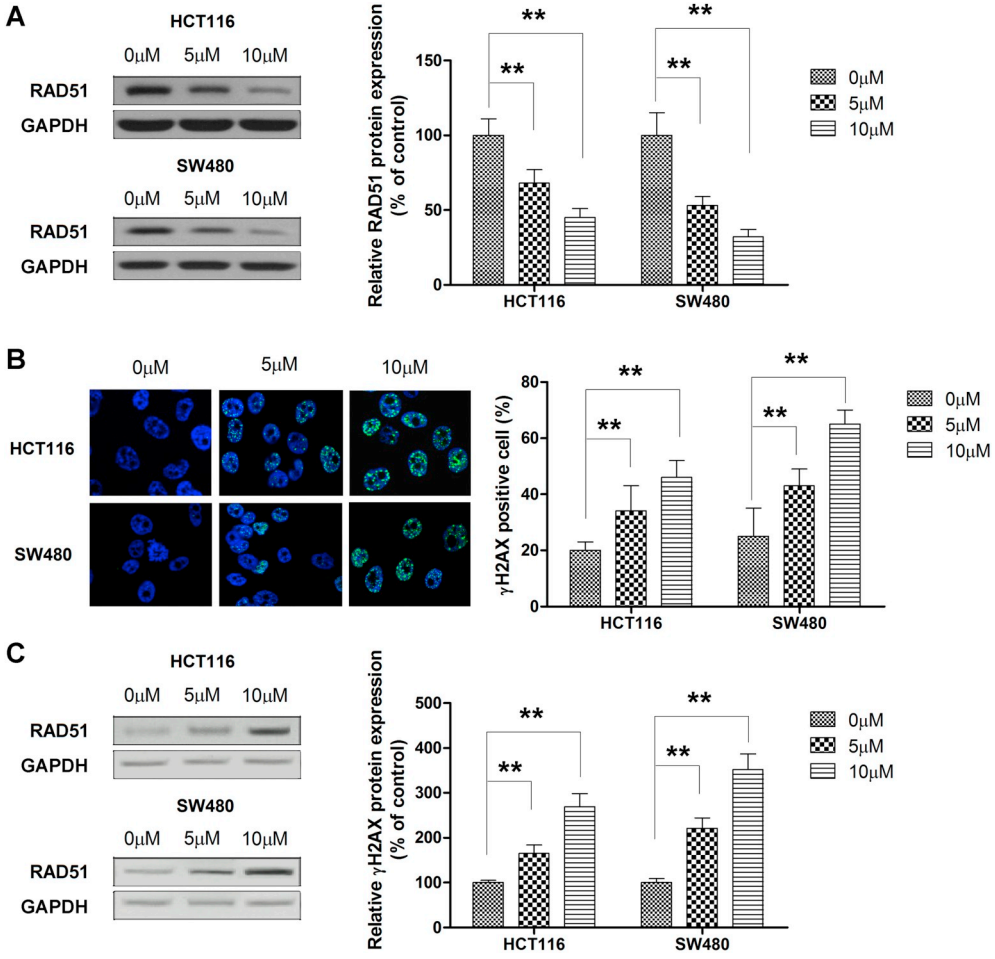

Fig. 4. AIF downregulated RAD51 and upregulated γH2AX in CRC cell lines. (A, C). Western blots showing relative RAD51 and γH2AX levels in AIF-treated CRC cells, normalized to GAPDH. B. Number of γH2AX foci in the AIF-treated and control cells. Data are presented as mean ± SD from three independent experiments, $^{**}p < 0.01$.

3.5. RAD51 silencing augmented the effects of AIF in CRC cells

To further investigate whether RAD51 contributed to the anti-cancer effect of AIF against CRC cells, we silenced RAD51 expression using specific siRNA (Fig. 5A). In line with the results so far, AIF (10 μM) treatment decreased RAD51 protein levels in CRC cells (Fig. 5A). Furthermore, RAD51 knockdown significantly decreased γ-H2AX levels when compared with to the control siRNA-transfected cells, which was partly alleviated by AIF treatment (Fig. 5B). In addition, RAD1 knockdown also enhanced the anti-proliferative effect (Fig. 5C), as well as the apoptosis-inducing effects of AIF (Fig. 5D) in the HCT-116 and SW480 cells. Inhibition of RAD1 increased the percentage of apoptotic cells in the AIF-treated HCT-116 and SW480 cell lines from 21% and 28% to 30% and 44% respectively (Fig. 5D). Consistent with this, knockdown of RAD51 further augmented the effects of AIF on the expression levels of apoptosis-related proteins (Fig. 5E). Taken together, RAD51 is an important mediator of AIF-regulated cell growth and apoptosis in CRC.

3.6. Overexpression of RAD51 alleviated the effects of AIF in CRC cells

We further validated the role of RAD51 in the anti-cancer effects AIF by exogenously overexpressing RAD1 in the HCT-116 and SW480 cells (Fig. 6A), which was slightly reduced in the AIF-treated cells. RAD51 overexpression partially alleviated the increased γ-H2XA levels induced by AIF (Fig. 6B), as well as the latter's anti-proliferative effect on CRC cells (Fig. 6C). Furthermore, overexpression of RAD51 partly reversed AIF mediated apoptosis, and the levels of apoptosis-related proteins in CRC cells (Fig. 6D and E). These findings confirmed that AIF inhibited CRC cell growth by modulating RAD51 expression.

3.7. AIF suppresses tumor growth in CRC xenograft model

To explore the *in vivo* therapeutic effect of AIF on tumor growth, we established a CRC xenograft model by inoculating 1×10^7 HCT-116 cells into the left flanks of six week-old male athymic BALB/c nu/nu mice. Once the tumor volume reached approximately 100 mm^3, the

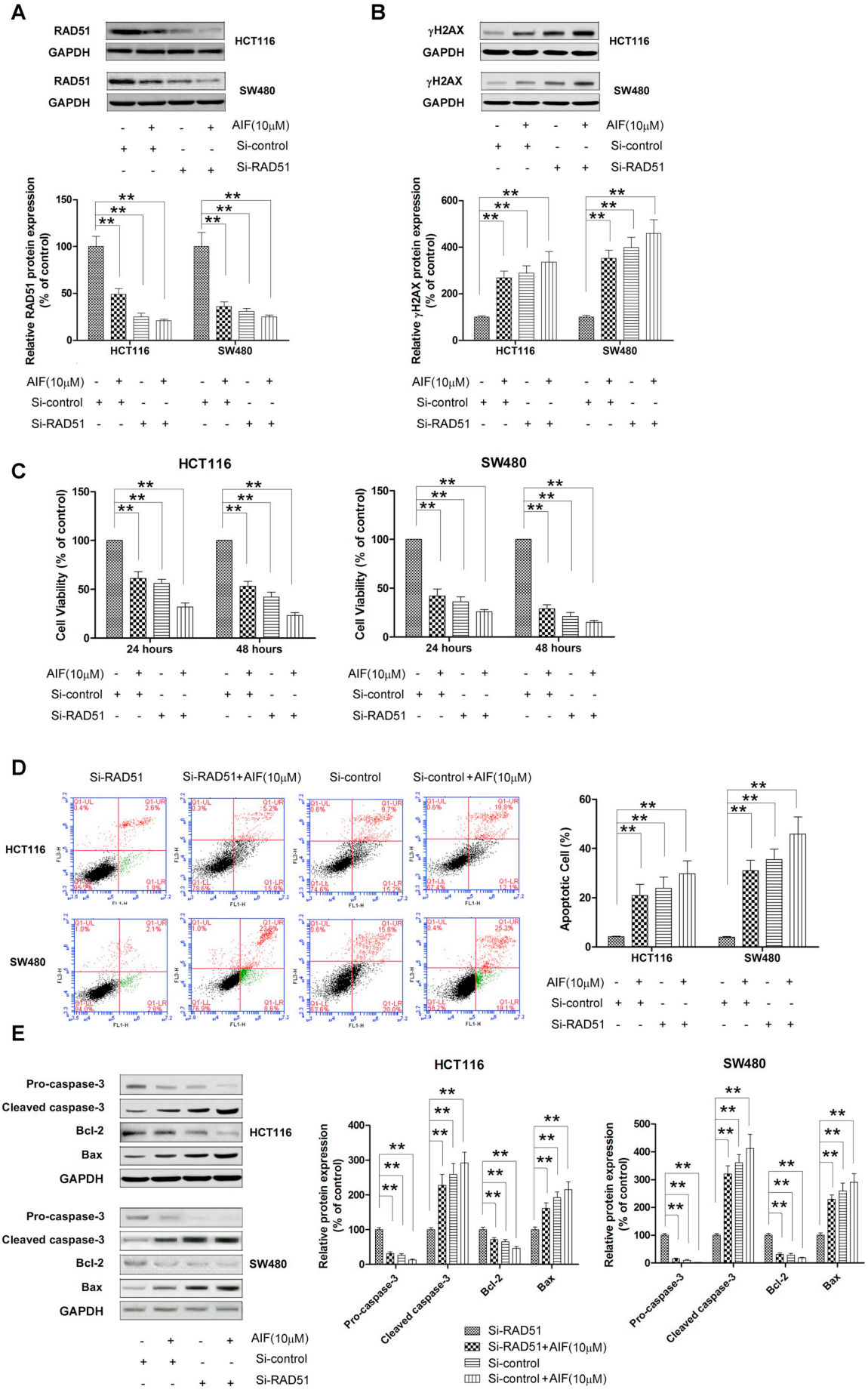

(caption on next page)

Fig. 5. Silencing RAD51 augmented the antitumor effect of AIF against CRC cells. HCT-116 and SW480 cells were transfected with RAD51 or control siRNA, and treated with 10 μM AIF 48 h later. (A, B). Western blots showing relative expression levels of RAD51 and γH2AX normalized to GAPDH. (C, D). Cell viability and apoptosis in each group were analyzed by CCK-8 assay and Annexin V/PI staining respectively. E. Western blots showing the relative expression of pro-caspase-3, caspase-3, Bcl-2, and Bax normalized to GAPDH. Data are presented as mean ± SD from three independent experiments, $^{**}p < 0.01$.

mice were respectively treated with the vehicle, 25 mg/kg or 50 mg/kg AIF daily for 24 days. As shown in Fig. 7A and B, the tumor size and weight on the 24th day were significantly lower in the AIF-treated mice compared to the control mice. Furthermore, no obvious changes were seen in the body weight of the mice of all groups, indicating lack of any systemic toxicity induced by AIF (Fig. 7E). Consistent with the *in vitro* findings, AIF treatment markedly increased the number of TUNEL-positive apoptotic cells in the tumor tissues in a dose-dependent manner, compared to the vehicle group (Fig. 7C). Likewise, AIF also downregulated the *in situ* levels of the proliferative marker Ki-67, the anti-apoptotic Bcl-2 and RAD51, and increased that of the pro-apoptotic cleaved caspase-3 and Bax in the tumor tissues (Fig. 7D). Thus, AIF retarded tumor growth by inhibiting proliferation and DNA repair, and inducing apoptosis. Finally, histological examination of heart, liver, spleen, lung and kidney tissues of the AIF-treated tumor bearing mice showed absence of any pathological signs in these vital organs (Fig. 7F). Taken together, AIF effectively suppressed CRC tumor growth without any adverse effects on normal tissues.

4. Discussion

Apoptosis, or programmed cell death, is the mechanism employed by most anti-cancer drugs to clear tumor cells. We found that AIF exposure significantly increased the percentage of apoptotic cells, and upregulated the pro-apoptotic proteins, in CRC cells. This is in agreement with the findings of Han et al. who reported that AIF induced apoptosis in ESSC cells *via* the inhibition of the miR-370/PIM signaling pathway [19]. Furthermore, Namkoong et al. demonstrated that AIF also induced lung tumor cell apoptosis by inhibiting the ERK/MAPK and NF-κB pathways [16]. Studies also show the potent radio-sensitizing effects of AIF in ESSC cells [15]. These findings indicate that AIF is a potent and pleiotropic anti-cancer drug candidate. In contrast to its effects on tumor cells, AIF shows an anti-apoptotic activity in non-tumor cells. Yin and Wang showed that AIF alleviated glucocorticoid-induced osteoporosis by preventing apoptosis in the osteoblasts and osteocytes [25,26]. Therefore, the effect of AIF on apoptosis depends on cell types and their pathological state.

Ionizing radiation and some chemical agents cause tumor cell death by inducing lethal DSB lesions. Occurrence of DNA damage activates the cNHEJ and HRR pathways which repair the DNA lesions and maintain genetic integrity [27]. AIF administration induced cell death in CRC cells, as well as downregulated RAD51, a key protein involved in HRR. We hypothesized therefore that AIF caused CRC cell death by inducing DNA damage and inhibiting the subsequent repair pathways. Consistent with this hypothesis, AIF treatment triggered DSB in CRC cells, as evidenced by the increase in γ-H2AX foci. Furthermore, silencing or overexpressing RAD51 respectively enhanced and abrogated the effects of AIF. Thus, AIF inhibited CRC cell growth by inducing DSB and blocking the repair process *via* RAD1 inhibition.

Aberrant overexpression of RAD51 has been observed in various malignancies like breast cancer, non-small-cell lung, and prostate cancer [28,29], and is significantly correlated to poor prognosis. Therefore, targeting RAD51 and reducing it to baseline levels may sensitize tumors cells to DNA damaging treatments. In line with our findings, Gasparini et al. demonstrated that miR-155 augmented radiotherapy outcome in breast cancer by targeting RAD51 and the DNA repair pathways [30]. In addition, small molecule RAD51 inhibitors, such as halenaquinone, B02, RI-1 and IBR2, enhanced the efficacy of radiotherapy and the DNA damaging effects of anti-cancer drugs [31]. Therefore, combining RAD51 inhibitors with AIF can potentially achieve a strong anti-neoplastic effect.

DSBs result in H2AX phosphorylation by ATM at ser-139, which subsequently recruits the DNA repair proteins like BRCA1, RAD50 and RAD51 to the lesion sites. AIF treatment increased γ-H2AX phosphorylation levels and the formation of γ-H2AX foci, indicating that AIF induced DNA damage in the CRC cells. Effective DNA repair enables the cancer cells to survive DNA damage induced by chemotherapeutic or radiotherapeutic treatments. Therefore, inhibiting DNA repair pathways is a promising therapeutic strategy for increasing the efficacy of such treatments. Our findings suggest that AIF can be used as an inhibitor of the DNA repair pathway either alone, or in combination with other chemotherapeutic agents.

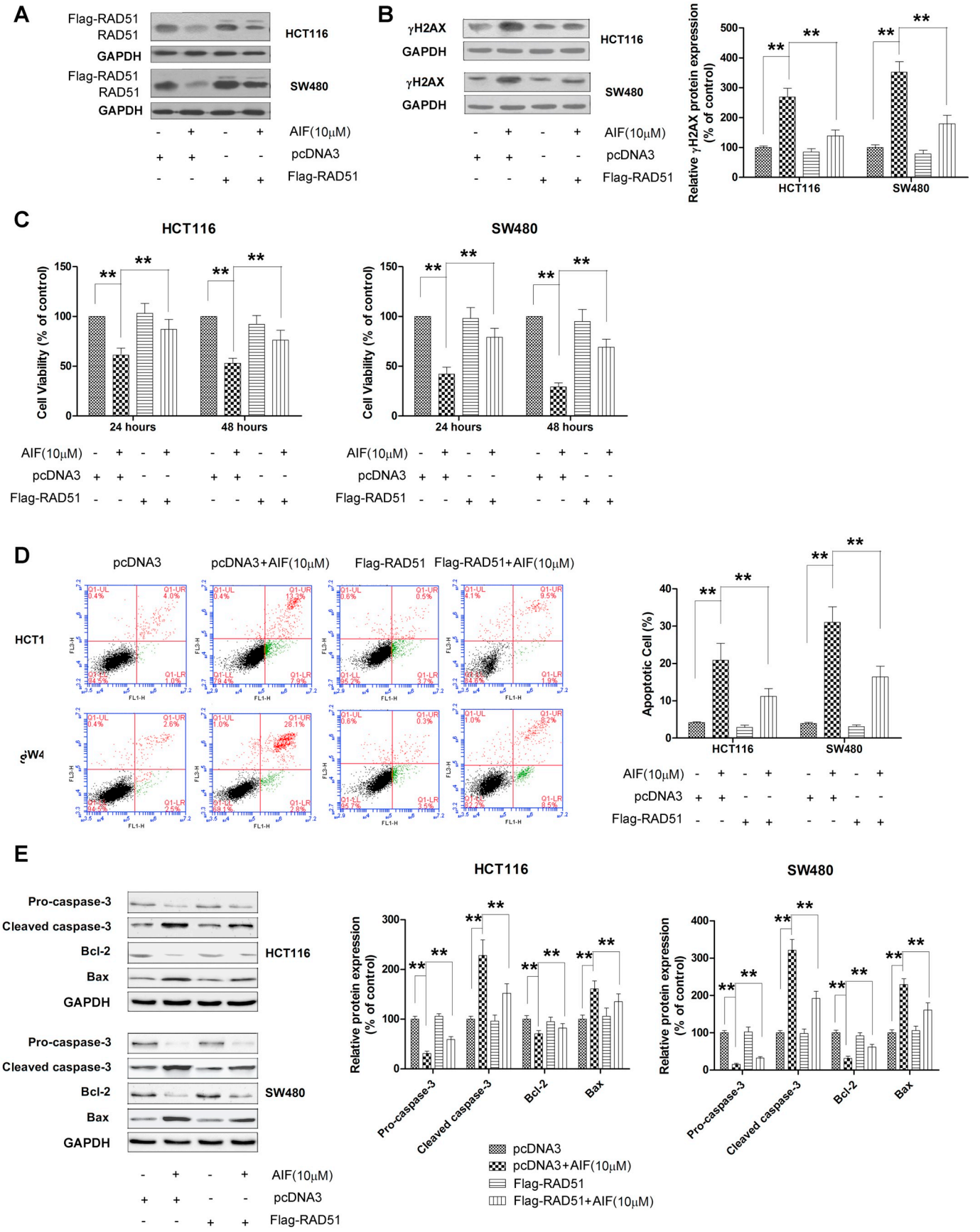

Fig. 6. Overexpression of RAD51 alleviates the anti-proliferative effect of AIF in CRC cells. HCT-116 and SW480 cells were transfected with Flag-RAD51 or pcDNA3 vector, and stimulated with 10 μM AIF after 48 h. (A, B). Western blots showing relative expression of RAD51 and γH2AX normalized to GAPDH. (C, D). Cell viability and apoptosis were analyzed by CCK-8 assay and Annexin V/PI staining respectively. E. Western blots showing relative expression of pro-caspase-3, caspase-3, Bcl-2, and Bax normalized to GAPDH. Data presented as mean ± SD from three independent experiments, $^{**}p < 0.01$.

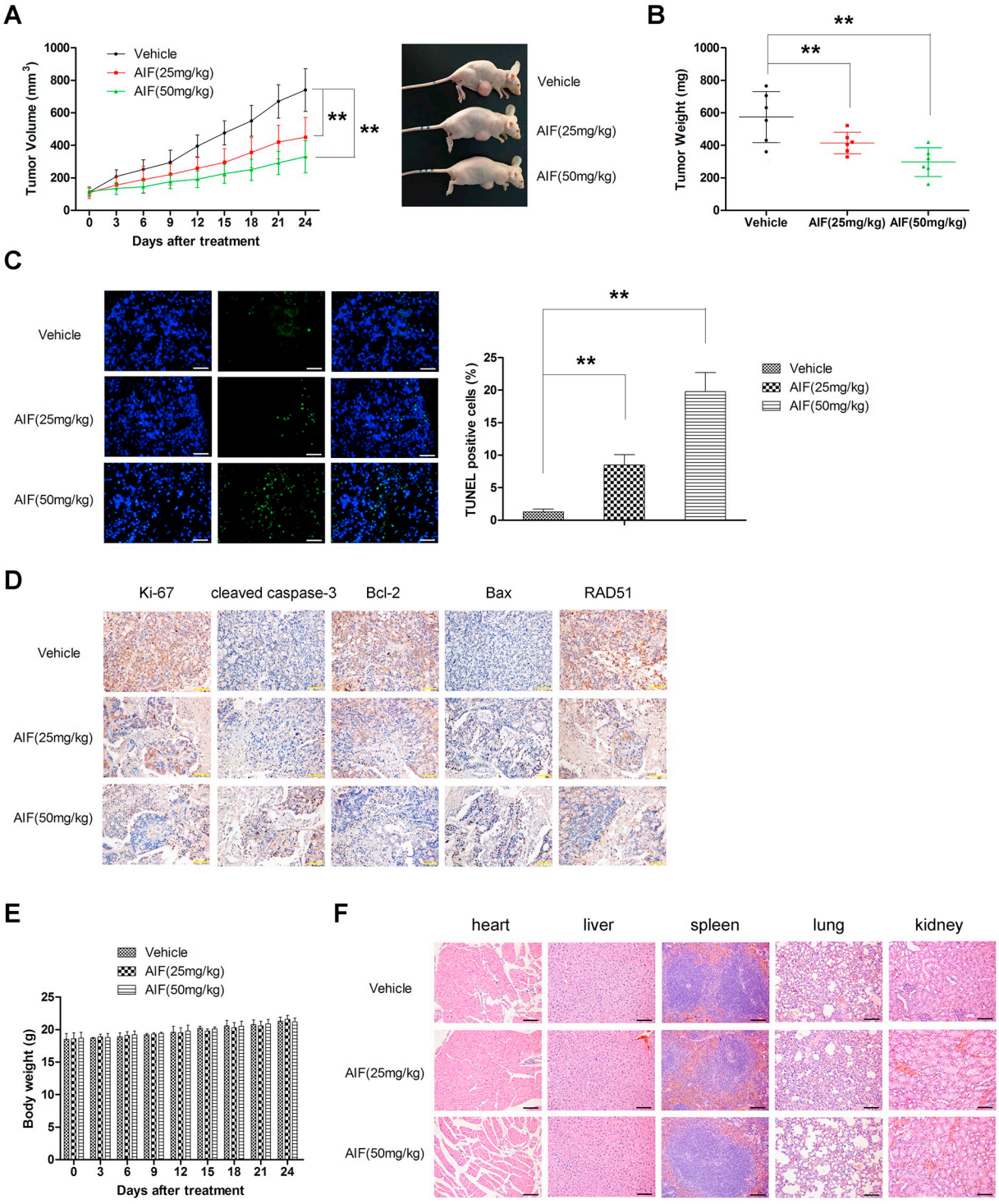

Fig. 7. AIF administration inhibits CRC progression in a HCT-116 xenograft model. Ten million HCT-116 cells were inoculated into the left flank of each nude mouse and AIF (25 and 50 mg/kg) or vehicle was administrated daily for 24 days *via* intraperitoneal injections. A. Tumor volume was measured twice a week and estimated according the formula ($V = 1/2 \times D \times d^2$), $^{**}p < 0.01$. B. Tumor weight was weighed after tumor dissection, $^{**}p < 0.01$. C. Representative picture of TUNEL stained tissue sections showing *in situ* apoptosis, $^{**}p < 0.01$. D. Representative pictures of IHC staining for Ki-67, cleaved caspase-3, Bcl-2, Bax and RAD51 in the xenograft tumor tissues. E. The body weight of mice in different treatment groups was recorded twice a week. F. Representative pictures of H&E stained tissues of the heart, liver, spleen, lung and kidney of the AIF-treated mice.

Funding

Beijing Medical Award Foundation (YYHYXKYJJ-216).

Declaration of conflicts

None.

Author contribution

Dong Li designed the research; Dong Li, Xiaoyan Li, Genqu Li, Yan Meng and Yanghong Jin performed experiments; Shuang Shang analyzed the data; Dong Li and Yanjie Li wrote the paper.

Appendix A. Supplementary data

Supplementary data to this article can be found online at https://doi.org/10.1016/j.lfs.2018.11.032.

References

[1] A. Jemal, et al., Global cancer statistics, CA Cancer J. Clin. 61 (2) (2011) 69–90.
[2] L.A. Torre, et al., Global cancer statistics, 2012, CA Cancer J. Clin. 65 (2) (2015) 87–108.
[3] S.P. Jackson, J. Bartek, The DNA-damage response in human biology and disease, Nature 461 (7267) (2009) 1071–1078.
[4] J.R. Chapman, M.R. Taylor, S.J. Boulton, Playing the end game: DNA double-strand break repair pathway choice, Mol. Cell 47 (4) (2012) 497–510.
[5] J.M. Mason, et al., The RAD51-stimulatory compound RS-1 can exploit the RAD51 overexpression that exists in cancer cells and tumors, Cancer Res. 74 (13) (2014) 3546–3555.
[6] V. Turinetto, C. Giachino, Multiple facets of histone variant H2AX: a DNA double-strand-break marker with several biological functions, Nucleic Acids Res. 43 (5) (2015) 2489–2498.
[7] F. Dona, et al., Loss of histone H2AX increases sensitivity of immortalized mouse fibroblasts to the topoisomerase II inhibitor etoposide, Int. J. Oncol. 33 (3) (2008) 613–621.
[8] S. Zha, et al., Complementary functions of ATM and H2AX in development and suppression of genomic instability, Proc. Natl. Acad. Sci. U. S. A. 105 (27) (2008) 9302–9306.
[9] C. Cabral, et al., Natural products as a source for new leads in cancer research and treatment, Evid. Based Complement. Alternat. Med. 2018 (2018) 8243680.
[10] A.L. Harvey, R. Edrada-Ebel, R.J. Quinn, The re-emergence of natural products for drug discovery in the genomics era, Nat. Rev. Drug Discov. 14 (2) (2015) 111–129.
[11] M.A. Mvondo, et al., Alpinumisoflavone and abyssinone V 4′-methylether derived from *Erythrina lysistemon* (Fabaceae) promote HDL-cholesterol synthesis and prevent cholesterol gallstone formation in ovariectomized rats, J. Pharm. Pharmacol. 67 (7) (2015) 990–996.
[12] J.R. Lyddiard, P.J. Whitfield, Inhibition of Site I mitochondrial electron transport by an extract of the seeds of *Millettia thonningii*: a potential mechanism for the plant's molluscicidal and schistosome larvicidal activity, J. Helminthol. 75 (3) (2001) 259–265.
[13] M.A. Mvondo, et al., Effects of alpinumisoflavone and abyssinone V-4′-methyl ether derived from *Erythrina lysistemon* (Fabaceae) on the genital tract of ovariectomized female Wistar rat, Phytother. Res. 26 (7) (2012) 1029–1036.
[14] J.C. Chukwujekwu, F.R. Van Heerden, J. Van Staden, Antibacterial activity of flavonoids from the stem bark of *Erythrina caffra* thunb, Phytother. Res. 25 (1) (2011) 46–48.
[15] B. Zhang, et al., Alpinumisoflavone radiosensitizes esophageal squamous cell carcinoma through inducing apoptosis and cell cycle arrest, Biomed. Pharmacother. 95 (2017) 199–206.
[16] S. Namkoong, et al., Alpinumisoflavone induces apoptosis and suppresses extracellular signal-regulated kinases/mitogen activated protein kinase and nuclear factor-kappaB pathways in lung tumor cells, Biol. Pharm. Bull. 34 (2) (2011) 203–208.
[17] T. Wang, et al., Alpinumisoflavone suppresses tumour growth and metastasis of clear-cell renal cell carcinoma, Am. J. Cancer Res. 7 (4) (2017) 999–1015.
[18] M. Gao, et al., Reduction of COX-2 through modulating miR-124/SPHK1 axis contributes to the antimetastatic effect of alpinumisoflavone in melanoma, Am. J. Transl. Res. 9 (3) (2017) 986–998.
[19] Y. Han, et al., Alpinumisoflavone induces apoptosis in esophageal squamous cell carcinoma by modulating miR-370/PIM1 signaling, Am. J. Cancer Res. 6 (12) (2016) 2755–2771.
[20] M.Q. Gao, et al., Hispidulin suppresses tumor growth and metastasis in renal cell carcinoma by modulating ceramide-sphingosine 1-phosphate rheostat, Am. J. Cancer Res. 7 (7) (2017) 1501–1514.
[21] H. Gao, et al., Hispidulin mediates apoptosis in human renal cell carcinoma by inducing ceramide accumulation, Acta Pharmacol. Sin. 38 (12) (2017) 1618–1631.
[22] N. Wang, et al., Euxanthone suppresses tumor growth and metastasis in colorectal cancer via targeting CIP2A/PP2A pathway, Life Sci. 209 (2018) 498–506.
[23] J.M. Adams, Ways of dying: multiple pathways to apoptosis, Genes Dev. 17 (20) (2003) 2481–2495.
[24] T.T. Paull, et al., A critical role for histone H2AX in recruitment of repair factors to nuclear foci after DNA damage, Curr. Biol. 10 (15) (2000) 886–895.
[25] J. Yin, L. Han, W. Cong, Alpinumisoflavone rescues glucocorticoid-induced apoptosis of osteocytes via suppressing Nox2-dependent ROS generation, Pharmacol. Rep. 70 (2) (2018) 270–276.
[26] Y. Wang, et al., Alpinumisoflavone protects against glucocorticoid-induced osteoporosis through suppressing the apoptosis of osteoblastic and osteocytic cells, Biomed. Pharmacother. 96 (2017) 993–999.
[27] A. Soni, et al., Inhibition of Parp1 by BMN673 effectively sensitizes cells to radiotherapy by upsetting the balance of repair pathways processing DNA double-strand breaks, Mol. Cancer Ther. 17 (10) (2018) 2206–2216.
[28] A.P. Wiegmans, et al., Rad51 supports triple negative breast cancer metastasis, Oncotarget 5 (10) (2014) 3261–3272.
[29] Y. Liu, et al., RAD51C is required for Holliday junction processing in mammalian cells, Science 303 (5655) (2004) 243–246.
[30] P. Gasparini, et al., Protective role of miR-155 in breast cancer through RAD51 targeting impairs homologous recombination after irradiation, Proc. Natl. Acad. Sci. U. S. A. 111 (12) (2014) 4536–4541.
[31] A. Ward, K.K. Khanna, A.P. Wiegmans, Targeting homologous recombination, new pre-clinical and clinical therapeutic combinations inhibiting RAD51, Cancer Treat. Rev. 41 (1) (2015) 35–45.